

SCIENTIFIC REPORTS



OPEN

Room temperature 90° phase-matching in zirconium and magnesium co-doped lithium niobate crystals

Tengfei Kong^{1,2}, Hongde Liu^{1,2}, Xinyu Ge¹, Da Qu^{1,2}, Shiguo Liu¹, Shaolin Chen², Ling Zhang², Yongfa Kong^{2,3,4}, Romano Rupp^{2,5} & Jingjun Xu^{1,2,4}

Laser has been widely used in many aspects, by now it is difficult to get each frequency that we want, and frequency conversion is an effective way to obtain different frequency laser through a nonlinear optical crystal. MgO-doped LiNbO₃ (Mg:LN) crystal has usually been used for second harmonic generation (SHG) through temperature-matching configuration with a stove, till now a room temperature 90° phase-matching is still lacking. Here we find that the SHG of Nd:YAG laser is achieved at 26.1 °C while the optical damage resistance is higher than 6.5 MW/cm² in the ZrO₂ and MgO co-doped LiNbO₃ (Zr,Mg:LN) crystal. Moreover, the monotonic decrease of phase-matching temperature is firstly found with the increase of doping concentration. These unusual properties may be attributed to the formation of Mg_{Li}⁺ + Zr_{Nb}⁺ defect pairs. Our work suggests that Zr,Mg:LN crystal may be an attractive candidate for nonlinear optical applications.

Miniature, compact and high-power all-solid-state blue-green lasers are widely applied in ocean exploration, medical treatment, optical communication and laser display, etc^{1–4}. As one of the most versatile optical crystals, lithium niobate (LiNbO₃, LN) plays a key role in the second harmonic generation (SHG) of blue-green light from near-infrared lasers owing to its large nonlinearity and capability of temperature-tuned noncritical phase matching (90° phase-matching)^{5–8}. Unfortunately, optical damage in LiNbO₃, also known as photorefractive effect, induced by modest intensities of visible light, sharply decreases the conversion efficiency and hinders its practical usage^{9,10}. A breakthrough came that the optical damage resistance of LiNbO₃ could be improved at least two orders of magnitude when 4.6 mol.% MgO was doped into^{11,12}. From then on, MgO-doped LiNbO₃ (Mg:LN) has become the often used material in frequency conversion, optical waveguide, optical parametric oscillation and terahertz source^{13–17}. But for infrared-to-visible nonlinear frequency conversion, the phase-matching temperature is usually above 100 °C, so a precise temperature-controlled stove is needed. The extra unit in the laser cavity can increase the complexity of the system and lead to the additional energy loss¹⁸. Besides, the elevated operating temperature will also reduce components reliability and shorten service life. Detailed investigations show that the phase-matching temperature of Mg:LN increases with increased MgO concentration, and reaches the maximum near the doping threshold, then decreases with further increased doping concentration¹⁹. Therefore, it is possible that phase matching achieves at room temperature (about 25 °C) with a high enough doping concentration of MgO, but such heavily doped Mg:LN crystal is hard to grow with high optical quality²⁰. Later, several ions such as Zn²⁺, In³⁺, Sc³⁺, and Hf⁴⁺ were also reported to have the same resistance against optical damage when doped into LiNbO₃, but just like Mg:LN, the efficient noncritical phase matching at room temperature is still a problem^{19,21–23}. Therefore, room temperature 90° phase-matching has always been a serious challenge for LiNbO₃ at present.

In recent years, ZrO₂-doped LiNbO₃ (Zr:LN) has attracted great attentions because of its high optical damage resistance in the visible and even ultraviolet region, low doping threshold (2.0 mol.%) and distribution coefficient

¹School of Physics, Nankai University, Tianjin, 300071, China. ²MOE Key Laboratory of Weak-Light Nonlinear Photonics and TEDA Institute of Applied Physics, Nankai University, Tianjin, 300457, China. ³R&D Center, Taishan Sports Industry Group, Leling, 253600, China. ⁴Collaborative Innovation Center of Chemical Science and Engineering (Tianjin), Tianjin, 300072, China. ⁵Vienna University, Faculty of Physics, A-1090, Wien, Austria. Correspondence and requests for materials should be addressed to H.L. (email: liuhd97@nankai.edu.cn) or Y.K. (email: kongyf@nankai.edu.cn) or J.X. (email: jjxu@nankai.edu.cn)

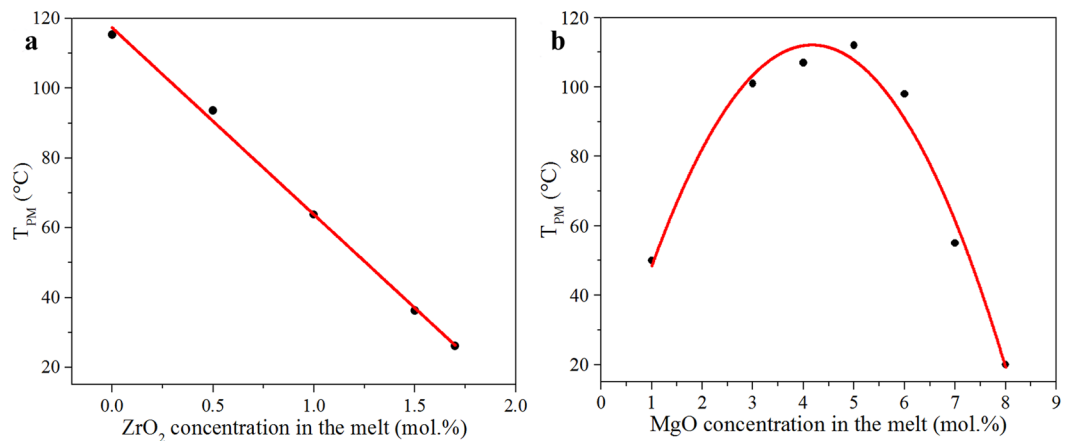


Figure 1. Phase-matching temperature T_{PM} versus the doping concentration in the melt of (a) Zr,Mg:LN and (b) Mg:LN crystals. The dotted symbols represent the experimental data, and the red guided line is a function fitting.

close to one^{24–26}. Up to now, investigations on Zr:LN crystals mainly focus on optical waveguide, defect structure and co-doping with photorefractive impurities^{27–29}, but their refractive indices and nonlinear optical properties (e.g., phase-matching temperature) are rarely reported. In fact, no sign of phase matching in Zr:LN crystals was found when they were heated from room temperature to above 200 °C in our pre-experiments, which implies that the phase-matching temperature of Zr:LN crystals may be lower than room temperature. If that is true, we may obtain room temperature 90° phase-matching by doubly doping with ZrO₂ and MgO in LiNbO₃. And co-doping with two optical damage resistant ions is conducive to finely tune the optical properties of LiNbO₃^{19,30}.

In this paper, we grew a series of ZrO₂ and MgO co-doped LiNbO₃ (Zr,Mg:LN) crystals with various ZrO₂ dopants, and the doping concentration of MgO was chosen as 5.0 mol.% because Mg:LN has high phase-matching temperature in this doping level. Our experimental results demonstrate that the phase-matching temperature of Zr,Mg:LN monotonically decreases with increased ZrO₂ concentration. And the efficient 90° phase-matching is achieved in Zr,Mg:LN crystal at room temperature without a stove, meanwhile it also has a very high optical damage resistance.

Results

Temperature tuned 90° phase-matching. Temperature tuned 90° phase-matching was achieved by using a Q-switched Nd:YAG laser with a wavelength of 1064 nm. The dependence of the phase-matching temperature T_{PM} on the ZrO₂ concentration in the melt for Zr,Mg:LN crystals is depicted in Fig. 1(a). From this figure, we can see that the T_{PM} decreases as the ZrO₂ concentration increases, and a straight line can be fitted well to the experimental data. For comparison, the T_{PM} versus the doping concentration of MgO for Mg:LN crystals is presented in Fig. 1(b), and the data are referenced from the previous literature¹⁹. The relationship between the T_{PM} and the impurity concentration is similar to a parabola going downwards, and the maximum temperature stays within the concentration range of 4~6 mol.%. Generally, the T_{PM} versus the doping concentration exposes a more or less expressed threshold behavior corresponding to the sharp change of optical properties, and this similar behavior can be found in other mono or dual doped LN crystals, such as Zn:LN²¹, Sc:LN²² and Zn,In:LN³⁰. In contrast, Zr,Mg:LN crystals exhibit a significant monotonic, and a simple linear extrapolation from existing data holds over a wider concentration range.

Please note that the phase-matching temperature in Zr_{1.7}Mg_{5.0}:LN crystal is 26.1 °C, which is close to room temperature (25 °C). Figure 2 clearly shows its normalized temperature-tuning curve for doubling 1064 nm using 90° phase-matching. The dots are the measured second harmonic output power, and the solid curve is a fit to the sinc(x) function, which almost perfectly overlaps the experimental data. The full width at half maximum (FWHM) of the temperature-tuning curve is 1.2 °C. Moreover, the conversion efficiency is plotted as a function of the incident fundamental power density in Fig. 3. An average second harmonic power of 91.5 mW is obtained with a conversion efficiency of 28.6% at the peak-power density of 50 MW/cm², and maintaining this conversion efficiency for two hours, there is no significant degradation. Overall, we should point out emphatically that if considering the temperature increase (about 2~3 °C) in the continuous harmonic output^{31,32}, Zr_{1.7}Mg_{5.0}:LN crystal is particularly well-suited for practical application of laser frequency doubling at room temperature.

Optical damage resistance. In order to measure the optical damage resistance, the distortion of the transmitted light beam through the wafer was observed with a 532 nm laser. Figure 4 shows the transmitted laser beam spots after 5 min of irradiation. As the concentration of ZrO₂ increases from 0.5 to 1.7 mol.%, none of Zr,Mg:LN crystals appears noticeable beam smeared, even under the highest focused intensity of 6.5×10^6 W/cm² in our laboratory, and the optical damage resistance is the same magnitude as that of Zr_{2.0}:LN. However, Mg_{5.0}:LN crystal can only withstand a maximum intensity of 4.1×10^5 W/cm² under the same conditions. The above results indicate that the optical damage resistance of these Zr,Mg:LN crystals is improved by at least an order of magnitude than that of Mg_{5.0}:LN.

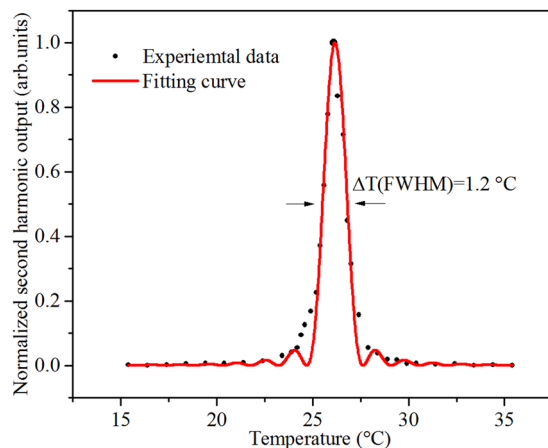


Figure 2. Normalized temperature-tuning curve for 90° phase-matching at 1064 nm in $\text{Zr}_{1.7}\text{Mg}_{5.0}\text{:LN}$ crystal. The dots are the measured second harmonic output at 532 nm, and the solid curve is fitted to $\text{sinc}(x) = (\sin(x)/x)^2$. The noncritical phase matching occurs at 26.1 °C with a FWHM of 1.2 °C.

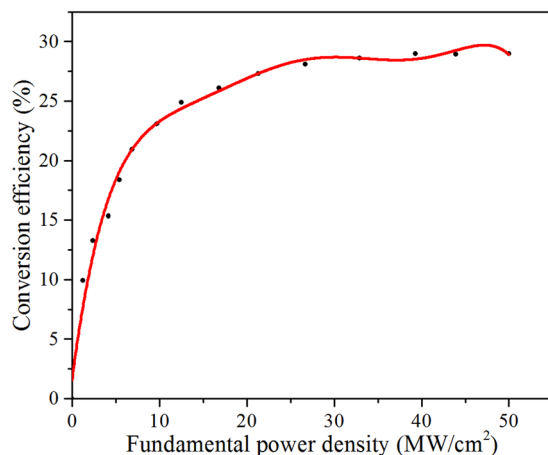


Figure 3. Power conversion efficiency of 90° phase-matched $\text{Zr}_{1.7}\text{Mg}_{5.0}\text{:LN}$ crystal as a function of the incident 1064 nm peak-power density. The solid curve is the guide to the eye.

To quantitatively characterize the optical damage resistance, the light-induced changes of the refractive index Δn of these crystals were measured by two-beam holography³³. Two *e*-polarized coherent beams at 532 nm were intersected in the wafers with equal intensity of 400 mW/cm². The change of refractive index Δn was calculated by the equation³⁴ $\eta_{\text{max}} = \sin^2(\pi d \Delta n / \lambda \cos \theta_{\text{cry}})$. Here, η_{max} is the maximum diffraction efficiency; λ is the wavelength, 532 nm; d is the crystal thickness, 3.0 mm; and θ_{cry} is the intersection half-angle of the two coherent beams outside the crystal, $2\theta_{\text{cry}} = 30^\circ$. The photoconductivity σ_{ph} was also estimated through the relationship, $\sigma_{\text{ph}} = \varepsilon_0 \varepsilon / \tau_e$, where ε_0 is the vacuum dielectric constant, $\varepsilon = 28$ is the relative dielectric constant of the crystal³⁵, and the erasure time constant τ_e is defined as the time when the diffraction efficiency decays to $1/e$ of its initial value.

The change of refractive index Δn and the photoconductivity σ_{ph} versus the ZrO_2 concentration for all samples are presented in Fig. 5. We can see that the change of refractive index reduces rapidly with doping 0.5 mol.% ZrO_2 into $\text{Mg}_{5.0}\text{:LN}$, then changes slightly as the ZrO_2 concentration increases. Moreover, the Δn of Zr,Mg:LN is considerably less than that of $\text{Mg}_{5.0}\text{:LN}$ and even lower than that of $\text{Zr}_{2.0}\text{:LN}$. In addition, the σ_{ph} of Zr,Mg:LN is larger than that of $\text{Mg}_{5.0}\text{:LN}$ but close to that of $\text{Zr}_{2.0}\text{:LN}$. It is well known that the increase of the photoconductivity is primarily responsible for the increase of the optical damage resistance³⁶. Therefore, the results demonstrate again that adding some ZrO_2 into $\text{Mg}_{5.0}\text{:LN}$ can further enhance the optical damage resistance, which is consistent with the results of the transmitted light beam distortion.

Infrared absorption spectra. The infrared absorption spectra, referring mainly to OH^- absorption spectra, sensitively reflect the change of defect structure in LiNbO_3 , which have become an important tool in studying the properties of dopant-related defects. Figure 6 shows the OH^- absorption spectra of CLN and Zr,Mg:LN crystals. As no obvious OH^- band shift is observed, a three-peak model³⁷ is employed by Lorentz fitting, and the results are listed in Table 1. For comparison, that of $\text{Mg}_{5.0}\text{:LN}$ and $\text{Zr}_{2.0}\text{:LN}$ crystals are also listed. It can be seen from the

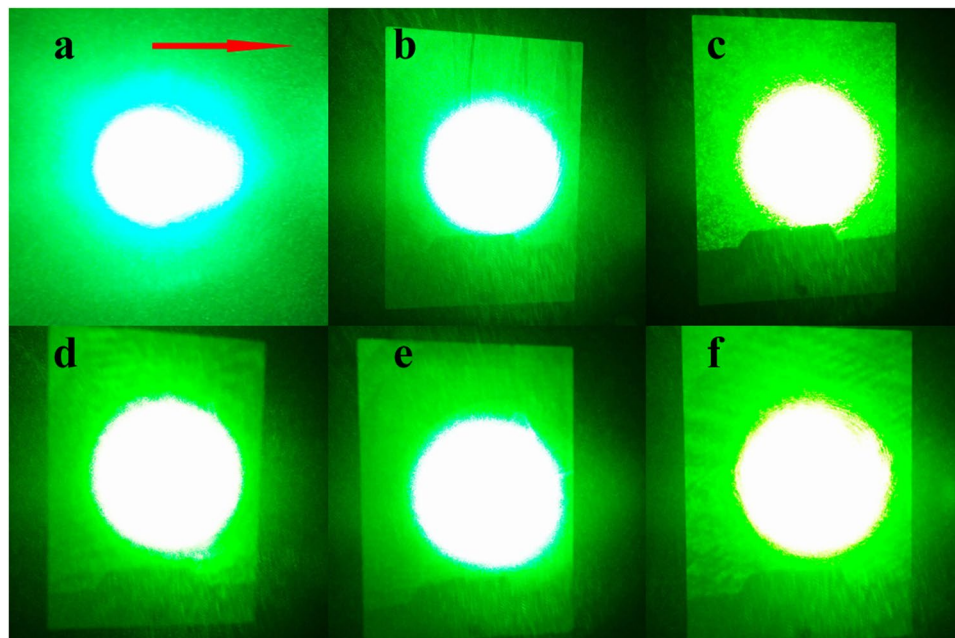


Figure 4. Transmitted laser beam spots after 5 min of irradiation. (a) $\text{Mg}_{5.0}:\text{LN}$, (b) $\text{Zr}_{0.5}\text{Mg}_{5.0}:\text{LN}$, (c) $\text{Zr}_{1.0}\text{Mg}_{5.0}:\text{LN}$, (d) $\text{Zr}_{1.5}\text{Mg}_{5.0}:\text{LN}$, (e) $\text{Zr}_{1.7}\text{Mg}_{5.0}:\text{LN}$, (f) $\text{Zr}_{2.0}:\text{LN}$. The light intensities are (a) $4.1 \times 10^5 \text{ W/cm}^2$ and (b)–(f) $6.5 \times 10^6 \text{ W/cm}^2$. The arrow direction represents the c -axis of the crystal.

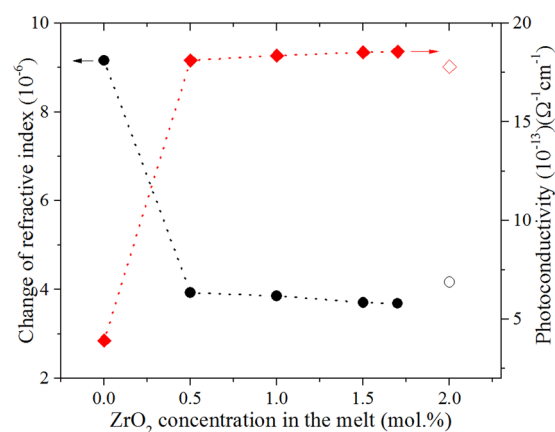


Figure 5. The change of refractive index Δn and photoconductivity σ_{ph} as a function of the ZrO_2 concentration in the melt for $\text{Zr,Mg}:\text{LN}$ crystals. The open symbols represent the data of $\text{Zr}_{2.0}:\text{LN}$ for comparison.

table that the component peaks of $\text{Zr}_{2.0}:\text{LN}$ are located at 3475, 3485, and 3495 cm^{-1} , respectively, which agree with the previous results³⁸, and the shift in component peaks is connected with the formation of $\text{OH}^- - \text{Zr}_{\text{Nb}}^-$ clusters. Moreover, with increased doping concentration of ZrO_2 , the relative intensity of $\text{OH}^- - \text{Zr}_{\text{Nb}}^-$ band will increase³⁹. As shown in the table, the peak of 3476 cm^{-1} appears in $\text{Zr}_{0.5}\text{Mg}:\text{LN}$ and moves to 3478 cm^{-1} with increased concentration of ZrO_2 . Based on these analyses, the total content of 0.5 mol.% ZrO_2 and 5.0 mol.% MgO in LiNbO_3 has reached the doping threshold.

UV-visible absorption spectra. The UV absorption edge of LiNbO_3 is sensitive to the crystal composition and defect⁴⁰, especially the absorption edge has a maximum violet-shift when the doping concentration reaches the threshold. The UV-visible absorption spectra of $\text{Zr,Mg}:\text{LN}$ crystals are shown in Fig. 7. The inset clearly shows the position of absorption edges. Here, the absorption edge is defined as the wavelength where the absorption coefficient is equal to 20 cm^{-1} . From this figure, we can see that the absorption edge of $\text{Zr}_{0.5}\text{Mg}_{5.0}:\text{LN}$ crystal has a maximum violet-shift, and with the doping concentration of ZrO_2 increasing from 0.5 to 1.7 mol.%, the absorption edge has an obvious red-shift. Therefore, we can conclude that the total doping concentration of 0.5 mol.% ZrO_2 and 5.0 mol.% MgO in LiNbO_3 reaches the threshold level, which is in agreement with the results of OH^- absorption spectra.

Sample	Position of peaks (cm^{-1})		
CLN	3468	3481	3490
Mg _{5.0} :LN		3535	
Zr _{2.0} :LN	3475	3485	3495
Zr _{0.5} Mg _{5.0} :LN	3476	3484	3493
Zr _{1.0} Mg _{5.0} :LN	3477	3485	3493
Zr _{1.5} Mg _{5.0} :LN	3478	3495	
Zr _{1.7} Mg _{5.0} :LN	3478	3487	3495

Table 1. The position of component peaks of the OH⁻ absorption spectra.

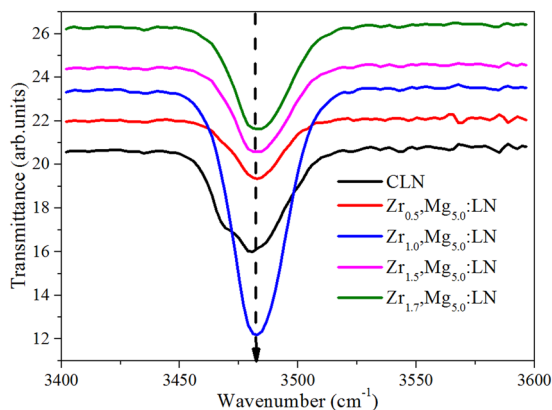


Figure 6. The OH⁻ absorption spectra of Zr,Mg:LN crystals. For comparison, that of CLN is also drawn. The dashed arrow marks the position of absorption peaks.

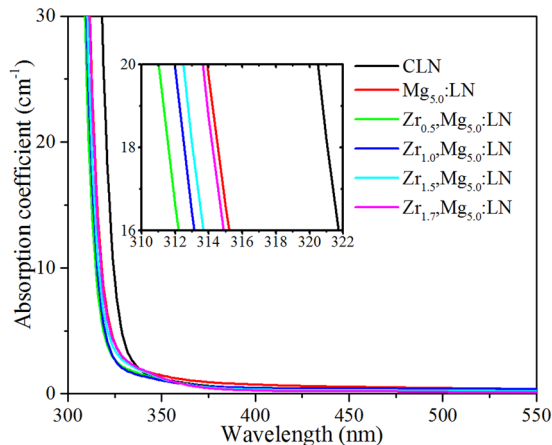


Figure 7. The UV-visible absorption spectra of Zr,Mg:LN crystals and of CLN and Mg_{5.0}:LN for comparison.

Discussion

The absorption spectra of Zr,Mg:LN crystals demonstrate that the total content of 0.5 mol.% ZrO₂ and 5.0 mol.% MgO has reached the doping threshold, which implies that impurity ions enter normal Nb sites after all Nb_{Li}⁴⁺ ions have been substituted. Moreover, the three-peak fitting analysis of OH⁻ absorption spectra indicates that the peak shifts are related to the formation of OH⁻-Zr_{Nb}⁻ complexes, and 3535 cm⁻¹ absorption peak³⁶ attributed to the OH⁻ stretching vibration of Mg_{Li}⁺-OH⁻-Mg_{Nb}³⁻ complex is not observed. These results indicate that the additional ZrO₂ can directly influence the threshold level of MgO, namely, Zr⁴⁺ ions affect the site occupation of Mg²⁺ ions. So it can be deduced that the appearance of Mg_{Li}⁺ + Zr_{Nb}⁻ neutral pairs leads to no obvious OH⁻ absorption band shift. And the amount of Mg_{Li}⁺ + Zr_{Nb}⁻ complexes will increase with increased concentration of ZrO₂. Considering the Mg_{Li}⁺ + Zr_{Nb}⁻ pairs without charge compensation, electron trap centers will dramatically reduce in crystals, which brings about the great increase of photoconductivity then results in strong optical damage resistance.

Our results on SHG of Nd:YAG lasers have shown that the additional ZrO₂ doping can significantly influence the phase-matching temperature of Mg_{5,0}:LN. In particular, the monotonic decrease of phase-matching temperature on ZrO₂ concentration is found for the first time, which is different from the previous reports on doped LiNbO₃. As we know, so-called optical damage resistant impurities in visible region such as Mg, Zn, In and Hf can enhance the UV photorefractive effect^{41,42}, but Zr exhibits excellent optical damage resistance in both visible and UV region. It is thought that the enhanced UV photorefractive effect has direct relationship with doped ions occupying Nb sites⁴³, which means that Zr⁴⁺ ions in Nb sites can greatly alter defect structures and properties of LiNbO₃. In Zr,Mg:LN crystals, Mg_{Li}⁺ + Zr_{Nb}⁻ neutral pairs may play an important role in this monotonic decrease relationship. However, further investigation is greatly needed to clarify the micro-mechanism.

Conclusion

We grew a series of LiNbO₃ co-doping with 5.0 mol.% MgO and various ZrO₂ concentrations. The experimental results indicate that the phase-matching temperature of Zr,Mg:LN decreases with increased ZrO₂ concentration for the first time. And 90° phase-matching of 1064 nm radiation is achieved at room temperature in Zr_{1,7}Mg_{5,0}:LN crystal, while it holds a high resistance of optical damage at 532 nm, and does not suffer any dark trace damage when exposed to high power laser irradiation for two hours, which will be greatly valuable for engineering applications in compact and efficient high-power green lasers. These excellent properties of Zr,Mg:LN may be attributed to the formation of Mg_{Li}⁺ + Zr_{Nb}⁻ neutral defect pairs.

Methods

Samples preparation. A series of doubly doped LiNbO₃ crystals were grown along the *c*-axis by the conventional Czochralski method in air. 0, 0.5, 1.0, 1.5 and 1.7 mol.% ZrO₂ were added, respectively, to the congruent melt (Li/Nb = 48.38/51.62) doping with 5.0 mol.% MgO, labeled as Mg_{5,0}:LN, Zr_{0,5}Mg_{5,0}:LN, Zr_{1,0}Mg_{5,0}:LN, Zr_{1,5}Mg_{5,0}:LN and Zr_{1,7}Mg_{5,0}:LN. After annealing treatment and artificial polarization, the crystals were cut into 3.0 mm and 1.0 mm thick *y*-plates for the characterization of photorefraction and absorption. Choosing crack-free and uniform bulk crystals were cut into 9.0 × 10.0 × 9.0 mm³ (X × Y × Z) for second harmonic generation, where *y*-axis was the transmission direction. All samples were optical grade polished on both faces perpendicular to *y*-axis of the crystal. For comparison, congruent LiNbO₃ and 2.0 mol.% ZrO₂-doped congruent LiNbO₃ crystals were also prepared, labelled as CLN and Zr_{2,0}:LN, respectively.

Spectra characterization. The infrared absorption spectra and UV-Visible absorption spectra of 1.0 mm thick *y*-plates were measured at room temperature with a Magna-560 Fourier transform infrared spectrophotometer and a U-4100 spectrophotometer, respectively. The resolution value of this infrared spectrometer was 4.0 cm⁻¹, and the step-length of the UV-Vis. spectrometer was 1.0 nm.

Second harmonic generation. The experiments for second harmonic generation were performed with a Q-switched Nd:YAG laser 1064 nm at a 1 Hz repetition rate, 8 ns pulse width. The laser facula diameter was 5.0 mm, and the maximum average output energy was 320 mJ. The fundamental light was directed to the crystal in a geometry with the *c*-axis of the crystal perpendicular to the polarization direction of the light, so-called 90° phase-matching. The second harmonic energy was detected with a band-pass filter and a pulse laser energy meter. The bulk crystal was mounted in an oven thermally controlled to a temperature better than ±0.2°C. The temperature was measured with a Pt-100 thermistor placed in direct contact with the crystal, and a slow heating rate was used about 0.5°C/min to minimize temperature gradients with the sample. In addition, the distance between the entrance and the exit windows of the crystal surfaces was at least 5.0 cm to minimize the possible temperature gradients along the crystal *y*-axis. The formula for the conversion efficiency was $\eta = E_2/E_1$, where E_1 was the energy of the fundamental wave and E_2 was that of the second harmonic wave.

Data availability. The datasets generated during the current study are available from the corresponding author on reasonable request.

References

- Xu, J. *et al.* Directly modulated green-light diode-pumped solid-state laser for underwater wireless optical communication. *Opt. Lett.* **42**, 1664–1667 (2017).
- Jensen, O. B. *et al.* 1.5 W green light generation by single-pass second harmonic generation of a single-frequency tapered diode laser. *Opt. Express* **17**, 6532–6539 (2009).
- Meier, T., Willke, B. & Danzmann, K. Continuous-wave single-frequency 532 nm laser source emitting 130 W into the fundamental transversal mode. *Opt. Lett.* **35**, 3742–3744 (2010).
- Jacquemet, M., Druon, F., Balembois, F., Georges, P. & Ferrand, B. Blue-green single-frequency laser based on intracavity frequency doubling of a diode-pumped ytterbium-doped laser. *Opt. Express* **13**, 2345–2350 (2005).
- Kauranen, M. P. Freeing nonlinear optics from phase matching. *Science* **342**, 1182–1183 (2013).
- Kang, Y. *et al.* Second-harmonic generation of a dual-frequency laser in a MgO:PPLN crystal. *Appl. Optics* **56**, 2968–2972 (2017).
- Getman, A. G., Popov, S. V. & Taylor, J. R. 7 W average power, high-beam-quality green generation in MgO-doped stoichiometric periodically poled lithium tantalate. *Appl. Phys. Lett.* **85**, 3026–3028 (2004).
- Wang, D. *et al.* Periodically poled self-frequency-doubling green laser fabricated from Nd:Mg:LiNbO₃ single crystal. *Opt. Express* **23**, 17727–17738 (2015).
- Ashkin, A. *et al.* Optically-induced refractive index inhomogeneities in LiNbO₃ and LiTaO₃. *Appl. Phys. Lett.* **9**, 72–74 (1966).
- Louchev, O. A., Hatano, H., Saito, N., Wada, S. & Kitamura, K. Laser-induced breakdown and damage generation by nonlinear frequency conversion in ferroelectric crystals: experiment and theory. *J. Appl. Phys.* **114**, 203101 (2013).
- Zhong, G., Jin, J. & Wu, Z. Measurements of optically induced refractive index damage of lithium niobate doped with different concentrations of MgO. *J. Opt. Soc. Am* **70**, 631–635 (1980).
- Furukawa, Y. *et al.* Photorefraction in LiNbO₃ as a function of [Li]/[Nb] and MgO concentrations. *Appl. Phys. Lett.* **77**, 2494 (2000).
- Takeya, K., Minami, T., Okano, H., Tripathi, S. R. & Kawase, K. Enhanced Cherenkov phase matching terahertz wave generation via a magnesium oxide doped lithium niobate ridge waveguide crystal. *APL Photon.* **2**, 016102 (2017).

14. Wang, L., Haunhorst, C. E., Volk, M. F., Chen, F. & Kip, D. Quasi-phase-matched frequency conversion in ridge waveguides fabricated by ion implantation and diamond dicing of MgO:LiNbO₃ crystals. *Opt. Express* **23**, 30188–30194 (2015).
15. Wang, Y. *et al.* Energy scaling and extended tunability of terahertz wave parametric oscillator with MgO-doped near-stoichiometric LiNbO₃ crystal. *Opt. Express* **25**, 8926–8936 (2017).
16. Tripathi, S. R. *et al.* Terahertz wave parametric amplifier. *Opt. Lett.* **39**, 1649–1652 (2014).
17. Hayashi, S. *et al.* Ultrabright continuously tunable terahertz-wave generation at room temperature. *Sci. Rep.* **4**, 5045 (2014).
18. Fan, T. Y., Cordova-Plaza, A., Digonnet, M. J. F., Byer, R. L. & Shaw, H. J. Nd:MgO:LiNbO₃ spectroscopy and laser devices. *J. Opt. Soc. Am. B* **3**, 140–148 (1986).
19. Volk, T., Rubiniina, N. & Wöhlecke, M. Optical-damage-resistant impurities in lithium niobate. *J. Opt. Soc. Am. B* **11**, 1681–1687 (1994).
20. Tan, H. *et al.* Segregation in MgO-doped congruent LiNbO₃. *J. Cryst. Growth* **142**, 111–116 (1994).
21. Volk, T. R., Pryalkin, V. I. & Rubiniina, N. M. Optical-damage-resistant LiNbO₃:Zn crystal. *Opt. Lett.* **15**, 996–998 (1990).
22. Yamamoto, J. K., Yamazaki, T. & Yamagishi, K. Noncritical phase matching and photorefractive damage in Sc₂O₃:LiNbO₃. *Appl. Phys. Lett.* **64**, 3228 (1994).
23. Kokanyan, E. P., Babajanyan, V. G., Demirkhanyan, G. G., Gruber, J. B. & Erdei, S. Periodically poled structures in doped lithium niobate crystals. *J. Appl. Phys.* **92**, 1544–1547 (2002).
24. Kong, Y. *et al.* Highly optical damage resistant crystal: zirconium-oxide-doped lithium niobate. *Appl. Phys. Lett.* **91**, 081908 (2007).
25. Liu, F. *et al.* High resistance against ultraviolet photorefractive in zirconium-doped lithium niobate crystals. *Opt. Lett.* **35**, 10–12 (2010).
26. Kokanyan, N., Chapron, D., Kokanyan, E. & Fontana, M. D. Zr doping on lithium niobate crystals: Raman spectroscopy and chemometrics. *J. Appl. Phys.* **121**, 095103 (2017).
27. Langrock, C. *et al.* Nonlinear diffusion model for annealed proton-exchanged waveguides in zirconium-doped lithium niobate. *Appl. Optics* **55**, 6559–6563 (2016).
28. Tian, T. *et al.* Fast UV-Vis photorefractive response of Zr and Mg codoped LiNbO₃:Mo. *Opt. Express* **21**, 10460–10466 (2013).
29. Zhang, D. *et al.* Zirconium-diffusion-doped Ti:LiNbO₃ strip waveguide for integrated optics. *Opt. Mater. Express* **5**, 1715 (2015).
30. Schlarb, U. *et al.* Refractive indices of Zn/In-co-doped lithium niobate. *Ferroelectrics* **185**, 269–272 (1996).
31. Kitamura, K., Hatano, H., Takekawa, S., Schütze, D. & Aono, M. Large pyroelectric effect in Fe-doped lithium niobate induced by a high-power short-pulse laser. *Appl. Phys. Lett.* **97**, 082903 (2010).
32. Zheng, S. *et al.* Pyroelectric effect in green light-assisted domain reversal of Mg-doped LiNbO₃ crystals. *Opt. Express* **20**, 29131–29136 (2012).
33. Lee, M. *et al.* Two-color hologram multiplexing from the colored state in stoichiometric LiNbO₃:Tb,Fe. *Appl. Phys. Lett.* **81**, 4511–4513 (2002).
34. Kogelnik, H. Coupled wave theory for thick hologram gratings. *Bell Syst. Tech. J.* **48**, 2909–2947 (1969).
35. Kokanyan, E. P., Razzari, L., Cristiani, I., Degiorgio, V. & Gruber, J. B. Reduced photorefractive in hafnium-doped single-domain and periodically poled lithium niobate crystals. *Appl. Phys. Lett.* **84**, 1880 (2004).
36. Bryan, D. A., Gerson, R. & Tomaschke, H. E. Increased optical damage resistance in lithium niobate. *Appl. Phys. Lett.* **44**, 847 (1984).
37. Kong, Y. *et al.* OH⁻ absorption spectra in doped lithium niobate crystals. *Phys. Lett. A* **196**, 128–132 (1994).
38. Xu, C. *et al.* Investigation on the OH⁻ absorption and blue photorefractive properties in Zr:Ru:Fe:LiNbO₃ crystals as a function of Li composition. *J. Opt. Soc. Am. B* **29**, 2814–2818 (2012).
39. Kovács, L. *et al.* Photorefractive damage resistance threshold in stoichiometric LiNbO₃:Zr crystals. *Opt. Lett.* **38**, 2861–2864 (2013).
40. Kovács, L. *et al.* Composition dependence of the ultraviolet absorption edge in lithium niobate. *Appl. Phys. Lett.* **70**, 2801 (1997).
41. Qiao, H. *et al.* Ultraviolet photorefractivity features in doped lithium niobate crystals. *Phys. Rev. B* **70**, 094101 (2004).
42. Xin, F. *et al.* Ultraviolet photorefractive at 325 nm in doped lithium niobate crystals. *J. Appl. Phys.* **107**, 033113 (2010).
43. Dong, Y. *et al.* Improved ultraviolet photorefractive properties of vanadium-doped lithium niobate crystals. *Opt. Lett.* **36**, 1779–1781 (2011).

Acknowledgements

This work was supported by the National Natural Science Foundation of China (11674179, 61705116), National Basic Research Program of China (2013CB328706), International Science & Technology Cooperation Program of China (2013DFG52660), Taishan Scholar Construction Project Special Fund and by Program for Changjiang Scholars and Innovative Research Team in University (IRT0149).

Author Contributions

Y.K., H.L. and J.X. conceived the study. S.L., L.Z. and T.K. contributed to crystal growth. S.C. and T.K. prepared the samples. T.K. performed the experiments. X.G. and D.Q. measured the spectra. R.R. discussed the results. T.K. and Y.K. wrote the manuscript. All authors reviewed the manuscript.

Additional Information

Competing Interests: The authors declare no competing interests.

Publisher's note: Springer Nature remains neutral with regard to jurisdictional claims in published maps and institutional affiliations.



Open Access This article is licensed under a Creative Commons Attribution 4.0 International License, which permits use, sharing, adaptation, distribution and reproduction in any medium or format, as long as you give appropriate credit to the original author(s) and the source, provide a link to the Creative Commons license, and indicate if changes were made. The images or other third party material in this article are included in the article's Creative Commons license, unless indicated otherwise in a credit line to the material. If material is not included in the article's Creative Commons license and your intended use is not permitted by statutory regulation or exceeds the permitted use, you will need to obtain permission directly from the copyright holder. To view a copy of this license, visit <http://creativecommons.org/licenses/by/4.0/>.

© The Author(s) 2018